Binding Energies and Linear and Nonlinear Optical Properties of a Donor Impurity in a Three-Dimensional Quantum Pseudodot

Muharrem Kirak[a] and Sait Yilmaz[b]

[a] Department of Science Education, Faculty of Education, Bozok University, 66200 Yozgat, Turkey

[b] Department of Physics, Faculty of Arts and Sciences, Bozok University, 66200 Yozgat, Turkey

Reprint requests to M. K.; E-mail: muharrem.kirak@bozok.edu.tr

Z. Naturforsch. **68a,** 744 – 750 (2013) / DOI: 10.5560/ZNA.2013-0053
Received December 5, 2012 / revised July 11, 2013 / published online September 18, 2013

A theoretical study of the electronic properties of the ground state and excited states and the linear and the third-order nonlinear optical properties (i. e., absorption coefficients and refractive indices) in a spherical GaAs pseudodot system is reported. The variational procedure has been employed in determining sublevel energy eigenvalues and their wave functions within the effective mass approximation. Our results indicate that the chemical potential of the electron gas and the minimum value of the pseudoharmonic potential have a great influence on the electrical and optical properties of hydrogenic impurity states. Also, we have found that the magnitudes of the absorption coefficient and the refractive index change of the spherical quantum dot increase for transitions between higher levels.

Key words: Quantum Pseudodot; Pseudoharmonic Potential; Hydrogenic Impurity; Nonlinear Optics.
PACS numbers: 73.21.La; 71.55.Eq; 42.65.-k

1. Introduction

The studies on nanostructures have gained great importance for both pure theoretical physics and applied science, therefore, there has been tremendous interest recently in semiconductor quantum dots (QDs). As we know, carrier confinement within QDs leads to quantization of the allowed energy levels. Hence, the electronic and optical properties of QDs are quite different from those of the bulk materials. From this point of view, these effects of quantum confinement which offer a wide range of potential applications for optoelectronic devices explain the origin of the interest. The impurity plays a fundamental role in a semiconductor QD due to influences both the electronic and optical properties of quantum devices. Several studies have been reported on the binding energies of the hydrogenic impurities in a spherical QD formed by different confining potentials, such as finite and infinite confining potentials [1 – 4], parabolic confinement potential [5 – 8], Woods–Saxon potential [9], Gaussian and modified Gaussian potentials [10, 11].

In the recent years, potential applications of semiconductor QDs in optoelectronic and photonic devices have motivated many authors to investigate on the linear and nonlinear optical properties of these structures [12 – 16]. There have been several theoretical studies on the optical absorption coefficient (AC) and refraction index change (RIC) associated with optical transitions (intersubband) in parabolic QDs [17 – 21]. In most previous studies, the harmonic oscillator potential is usually considered, since it has exact eigensolutions and matrix elements for various physical quantities [22]. Although this potential has some advantages, it is not realistic when compared to a real molecular vibrational potential [23]. A pseudoharmonic potential is commonly considered as anharmonic oscillator which is asymmetric about equilibrium distance r_0 and becomes infinite as $r \to 0$ [24]. So the nonlinear optical properties of QDs with pseudoharmonic potential have attracted much attention [25 – 29]. Very recently, the optical ACs and RICs of a donor impurity confined by a three-dimensional quantum pseudodot are studied by Xie and Chen [30]. Their calculations are made by using the matrix diagonalization method within the effective-mass approximation. In addition, Khordad [31] investigated the threshold frequency of absorption in a quantum pseudodot under the influence

of temperature and applied magnetic field. All of the above mentioned studies are concentrate on the calculation of the ACs and RICs for the transition between the lowest energy states, which is the transition $1s-1p$ between the ground state ($l=0$) and the first excited state ($l=1$). To our knowledge up to now, these optical properties have not been investigated for the transitions between higher energy states. The purpose of this paper is to investigate the linear and nonlinear optical properties of a donor impurity confined by a QD with a three-dimensional pseudoharmonic potential. In calculations, the variational scheme within the effective mass approximation has been used to determine the energy levels and their wave functions.

2. Theory

In the effective mass approximation, the Hamiltonian of a donor impurity with three-dimensional pseudoharmonic potential is given by

$$H=-\frac{\hbar^2}{2m^*}\nabla^2+V(r)-\frac{e^2}{4\pi\varepsilon_0\varepsilon r}. \tag{1}$$

Here, $\hbar$ is the Planck constant, m^* is the electronic effective mass in QD, r is the position of an electron, e is the electronic charge, and ε is the dielectric constant of the dot material. $V(r)$ is the three-dimensional pseudoharmonic potential having the form [32, 33]

$$V(r)=V_0\left(\frac{r}{r_0}-\frac{r_0}{r}\right)^2, \tag{2}$$

where V_0 is the chemical potential of the electron gas and r_0 is the minimum value of the pseudoharmonic potential. Substituting the wave function in the form $\psi_{nlm}(r,\theta,\phi)=R_{nl}(r)Y_l^m(\theta,\phi)$ into (1) with the absence of impurity, we obtain the radial part of (1) as

$$\frac{\mathrm{d}^2R_{nl}(r)}{\mathrm{d}r^2}+\frac{2}{r}\frac{\mathrm{d}R_{nl}(r)}{\mathrm{d}r}+\frac{2m^*}{\hbar^2}\left(E_{nl}-\frac{l(l+1)\hbar^2}{2m^*r^2}-V_0\left(\frac{r}{r_0}-\frac{r_0}{r}\right)^2\right)R_{nl}(r)=0, \tag{3}$$

where n, l, and m are the principal, orbital, and magnetic quantum numbers, respectively. The energy eigenvalue and eigenfunction of (3) are given in [33]:

$$E_{nl}=-2V_0+\frac{\hbar}{r_0}\sqrt{\frac{2V_0}{m^*}}\left((2n+1)+2\sqrt{\beta+\frac{1}{16}}\right) \tag{4}$$

and

$$R_{nl}(r)=Nr^{-\frac{1}{2}+2\sqrt{\beta+\frac{1}{16}}}\exp(-\alpha r^2)\cdot L_n^{2\sqrt{\beta+\frac{1}{16}}}(2\alpha r^2), \tag{5}$$

where N is the normalization constant and

$$\alpha^2=\frac{V_0}{r_0^2}\frac{m^*}{2\hbar^2},\quad \beta=\frac{m^*}{2\hbar^2}\left(V_0r_0^2+\frac{l(l+1)\hbar^2}{2m^*}\right). \tag{6}$$

The wave functions of the ground state ($n=0$, $l=0$, and $m=0$) and of the first ($n=1$, $l=1$, and $m=0$) and second ($n=2$, $l=2$, and $m=0$) excited states, respectively, in the absence of the impurity are

$$\psi_{000}=Nr^{-\frac{1}{2}+2\sqrt{\beta+\frac{1}{16}}}\exp(-\alpha r^2)\cdot L_0^{2\sqrt{\beta+\frac{1}{16}}}(2\alpha r^2)Y_0^0(\theta,\phi), \tag{7}$$

$$\psi_{110}=Nr^{-\frac{1}{2}+2\sqrt{\beta+\frac{1}{16}}}\exp(-\alpha r^2)\cdot L_1^{2\sqrt{\beta+\frac{1}{16}}}(2\alpha r^2)Y_1^0(\theta,\phi), \tag{8}$$

$$\psi_{220}=Nr^{-\frac{1}{2}+2\sqrt{\beta+\frac{1}{16}}}\exp(-\alpha r^2)\cdot L_2^{2\sqrt{\beta+\frac{1}{16}}}(2\alpha r^2)Y_2^0(\theta,\phi). \tag{9}$$

We assume that the trial wave functions of the ground state and the excited states for the case with the impurity are

$$\psi_\lambda=\psi_{nlm}(r,\theta,\phi)\exp(-\lambda r), \tag{10}$$

where λ is the variational parameter. The binding energy of a hydrogenic impurity is defined as

$$E_B=E_0(n,l)-E_{\mathrm{imp}}. \tag{11}$$

Here $E_0(n,l)$ and E_{imp} are the energy of the QD without and with the impurity, respectively. E_{imp} is determined by energy minimization with respect to the variational parameter λ by means of

$$E_{\mathrm{imp}}=\min_\lambda\frac{\langle\psi_\lambda|H|\psi_\lambda\rangle}{\langle\psi_\lambda|\psi_\lambda\rangle}, \tag{12}$$

where $\min_\lambda$ is the minimum of the expectation value of the Hamiltonian in (1). This quantity is found by varying the variational parameter.

Analytic forms for the linear $\alpha^{(1)}$ and third-order nonlinear ACs $\alpha^{(3)}(w,I)$ are given respectively by [17, 20]

$$\alpha^{(1)}(w) = w\sqrt{\frac{\mu}{\varepsilon_R}\frac{|M_{21}|^2\sigma_V\hbar\Gamma_{12}}{(E_{21}-\hbar w)^2+(\hbar\Gamma_{12})^2}} \tag{13}$$

and

$$\alpha^{(3)}(w,I) = -w\sqrt{\frac{\mu}{\varepsilon_R}}\left(\frac{I}{2\varepsilon_0 n_r c}\right) \cdot \frac{|M_{21}|^2\sigma_V\hbar\Gamma_{12}}{\left[(E_{21}-\hbar w)^2+(\hbar\Gamma_{12})^2\right]^2}\left[4|M_{21}|^2 - \frac{|M_{22}-M_{11}|^2\left[3E_{21}^2-4E_{21}\hbar w+\hbar^2(w^2-\Gamma_{12}^2)\right]}{E_{21}^2+(\hbar\Gamma_{12})^2}\right]. \tag{14}$$

The total AC is then given as

$$\alpha(w,I) = \alpha^{(1)}(w)+\alpha^{(3)}(w,I). \tag{15}$$

The linear $\Delta n^{(1)}(w)$ and third-order nonlinear $\Delta n^{(3)}(w,I)$ RICs are determined by [20, 26]

$$\frac{\Delta n^{(1)}(w)}{n_r} = \frac{\sigma_V}{2n_r^2\varepsilon_0}|M_{21}|^2\frac{(E_{21}-\hbar w)}{(E_{21}-\hbar w)^2+(\hbar\Gamma_{12})^2} \tag{16}$$

and

$$\frac{\Delta n^{(3)}(w,I)}{n_r} = -\frac{Ic}{4n_r^3\varepsilon_0}|M_{21}|^2 \cdot\left[\frac{\sigma_V I}{\left[(E_{21}-\hbar w)^2+(\hbar\Gamma_{12})^2\right]^2}\right] \cdot\left[4(E_{21}-\hbar w)|M_{21}|^2 - \frac{(M_{22}-M_{11})^2}{E_{21}^2+(\hbar\Gamma_{12})^2}\left\{(E_{21}-\hbar w)\cdot\left[E_{21}(E_{21}-\hbar w)-(\hbar\Gamma_{12})^2\right]-(\hbar\Gamma_{12})^2(2E_{21}-\hbar w)\right\}\right]. \tag{17}$$

Then the total RIC is given as

$$\frac{\Delta n(w,I)}{n_r} = \frac{\Delta n^{(1)}(w)}{n_r}+\frac{\Delta n^{(3)}(w,I)}{n_r}. \tag{18}$$

In the above equations, σ_V is the electron density, μ is the magnetic susceptibility, $\hbar w$ is the incident photon energy, c is the speed of light in free space, ε_0 is the dielectric permittivity of the vacuum, n_r is the refractive index of the dot material, $E_1(E_2)$ is the initial (final) state energy, $\Gamma_{12} = 1/\tau$ is the relaxation rate for states 1 and 2, τ is the relaxation time, $E_{21} = E_2 - E_1$ is the energy difference between two different electronic states, and I is the incident light intensity. M_{21} is the transition matrix element between the initial and final states and is defined as $M_{21} = \langle\psi_2|ez|\psi_1\rangle$. The matrix element is important for the calculation of different optical properties of the system related to electronic transitions. In highly symmetrical QDs, transitions from a lower state to an upper state are forbidden according to the selection rules. In spherical QDs, dipole transitions are allowed only between states satisfying the selection rules $\Delta l = \pm 1$, where l is the angular momentum quantum number [34]. We have chosen a polarized electromagnetic radiation in the z-direction.

3. Results and Discussion

In this section, we present numerical results of binding energies and optical properties of a GaAs spherical QD with pseudopotential. The atomic units have been used through the calculations, $\hbar = m_0 = e = 1$. The material parameters have been taken as following: The effective mass $m^* = 0.067m_0$ (m_0 is the mass of a free electron), $\varepsilon = 13.18$, $\sigma_V = 5.0\cdot 10^{24}$ m^{-3}, $n_r = 3.2$, and $\Gamma_{12} = 5.0$ ps^{-1}.

In Figure 1, the binding energies E_B of the ground state ($0s$), the first ($1p$) and second ($2d$) excited states are plotted as a function of dot radius for two different zero point parameters r_0 with $V_0 = 300$ meV. As

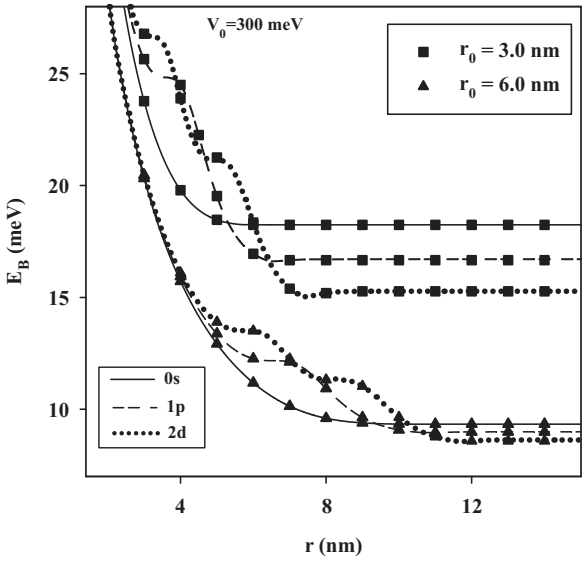

Fig. 1. Variation of the ground state ($0s$), the first ($1p$) and the second ($2d$) excited states binding energies with dot radius for two different values of zero point parameters ($r_0 = 3.0$ and 6.0 nm).

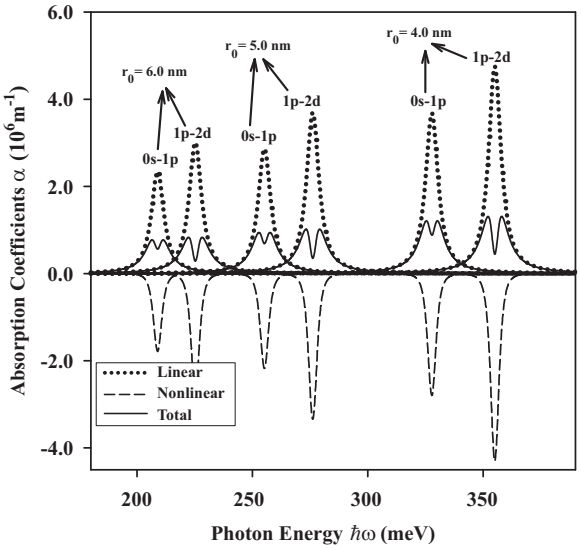

Fig. 2. Absorption coefficients of $0s-1p$ and $1p-2d$ transitions versus the incident photon energy $\hbar w$ for different zero point parameters ($r_0 = 4.0$, 5.0, and 6.0 nm) at $V_0 = 300$ meV and $I = 0.6\,\mathrm{MW/cm^2}$.

seen from Figure 1, for increasing dot radius, the binding energies for both the ground state and the excited states decrease and approach the bulk value for large dot sizes. Also, we observe that the binding energy of the ground state decreases more quickly than that of the excited states for the same r_0 value. In addition, the binding energy of the $r_0 = 3$ nm case is higher than that of the $r_0 = 6$ nm case. This physically means that with increasing r_0, the electron wave function becomes more splayed which leads to less binding of the donor electron. This result is consistent with Khordad's result [35]. We can also note that r_0 has more influence on higher energy levels. These results show that the effect of r_0 on the binding energies of the $0s$, $1p$, and $2d$ states of the hydrogenic impurity depends strongly on the quantum numbers n and l.

Figure 2 illustrates the ACs of $0s-1p$ and $1p-2d$ transitions versus the incident photon energy $\hbar w$ for three different zero point parameters ($r_0 = 4.0$, 5.0, and 6.0 nm). In this calculation, the chemical potential and the incident light intensity are taken as $V_0 = 300$ meV and $I = 0.6\,\mathrm{MW/cm^2}$, respectively. As shown in this figure, the linear AC is positive throughout the photon energy scale considered, whereas the third-order nonlinear optical AC term is negative. So the total AC is reduced by third-order nonlinear AC. All the ACs (absolute values of third-order coefficients) decrease with increasing r_0 for the $0s-1p$ and $1p-2d$ transitions. We know that the incident light energy equals to the energy difference between the levels. This energy is called resonance transition energy, which corresponds to the peak energy of the AC. We observe that the peak positions shift to lower photon energies (red shift) with r_0 increasing as the energy difference be-

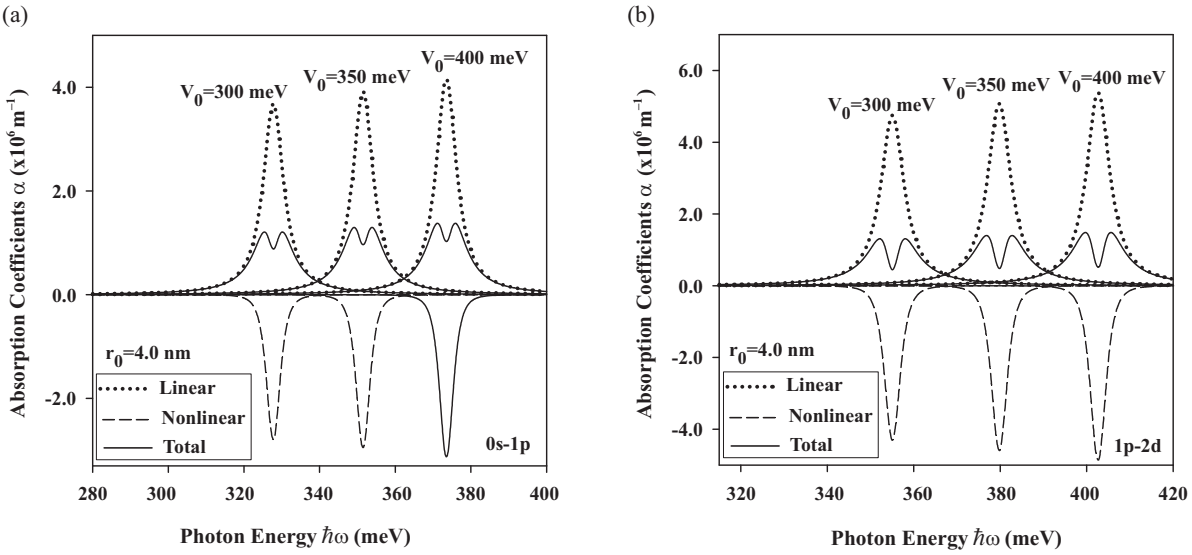

Fig. 3. Variation of ACs as a function of photon energy for various values of the chemical potential ($V_0 = 300$, 350, and 400 meV) at $r_0 = 4.0$ nm, $r = 7.0$ nm, and $I = 0.6\,\mathrm{MW/cm^2}$ for (a) $0s-1p$ and (b) $1p-2d$ transitions.

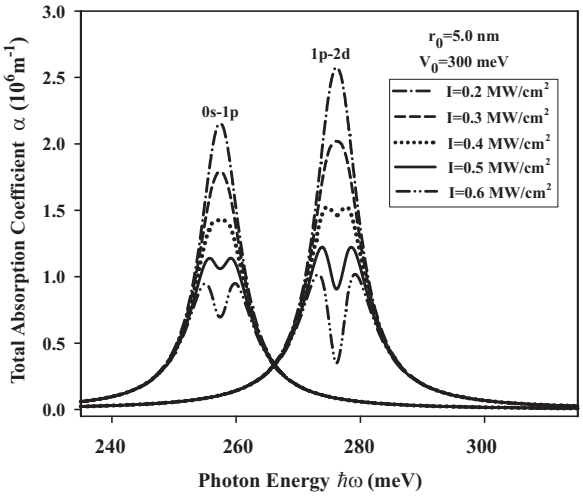

Fig. 4. Total ACs as a function of the photon energy for five different values of optical intensity ($I = 0.2$, 0.3, 0.4, 0.5, and 0.6 MW/cm^2) at $r_0 = 5.0$ nm, $r = 7.0$ nm and $V_0 = 300$ meV.

tween the electronic states decreases. Further we note that the amplitudes of the ACs for $1p-2d$ transition are much stronger than that of the $0s-1p$ transition. The reason for this situation is the increment in the electronic dipole transition matrix element, and the increment in the energy interval of two different electronic states shows that there exists an optical transition [20].

In Figure 3, in order to see the influence of the chemical potential V_0, we set $V_0 = 300$, 350, and 400 meV and plot the ACs as a function of photon energy with $I = 0.6$ MW/cm^2 for a) $0s-1p$ and b) $1p-2d$ transitions. It is clear that when V_0 increases, the peak positions shift to larger photon energies (blue shift) and the absorption peak moves to right. This behaviour can be explained with the fact that the wave function is more localized and the separation between the neighbouring energy levels becomes wider with increasing V_0. We should also mention that the total AC peak intensity increases due to the increasing of the electronic dipolar transition matrix elements with increasing V_0. These results are in agreement with the matrix diagonalization method results found in the literature [30].

The linear AC does not depend on the photon intensity I. However, the nonlinear AC depends on the intensity and so does the total AC. Figure 4 shows the total AC as a function of the incident photon energy for five different values of the optical intensity, $I = 0.2$, 0.3, 0.4, 0.5, and 0.6 MW/cm^2 with $r_0 = 5.0$ nm, $r = 7.0$ nm, and $V_0 = 300$ meV. The total AC reaches a maximum at a certain photon energy value, and this peak value reduces when the optical intensity increases. The absorption spectrum has been strongly bleached at sufficiently high optical intensities. When the difference between the magnitudes of the linear and the nonlinear ACs is small, the reso-

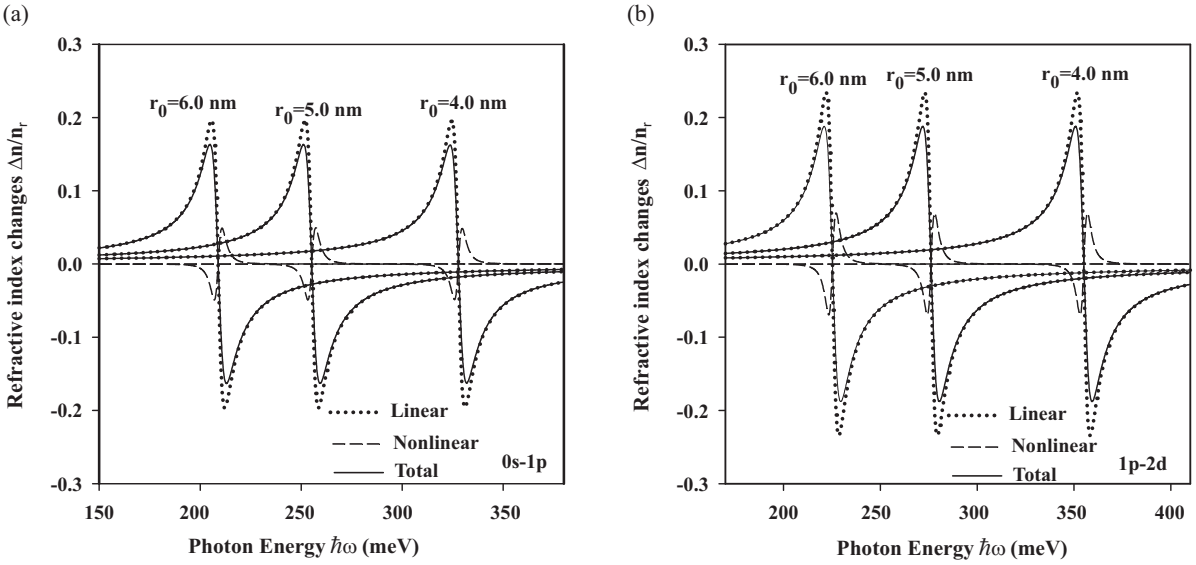

Fig. 5. Variation of the RIC as a function of the photon energy with different values of zero point parameters ($r_0 = 4.0$, 5.0, and 6.0 nm) at $V_0 = 300$ meV, $r = 7.0$ nm and $I = 0.6$ MW/cm^2 for (a) $0s-1p$ and (b) $1p-2d$ transitions.

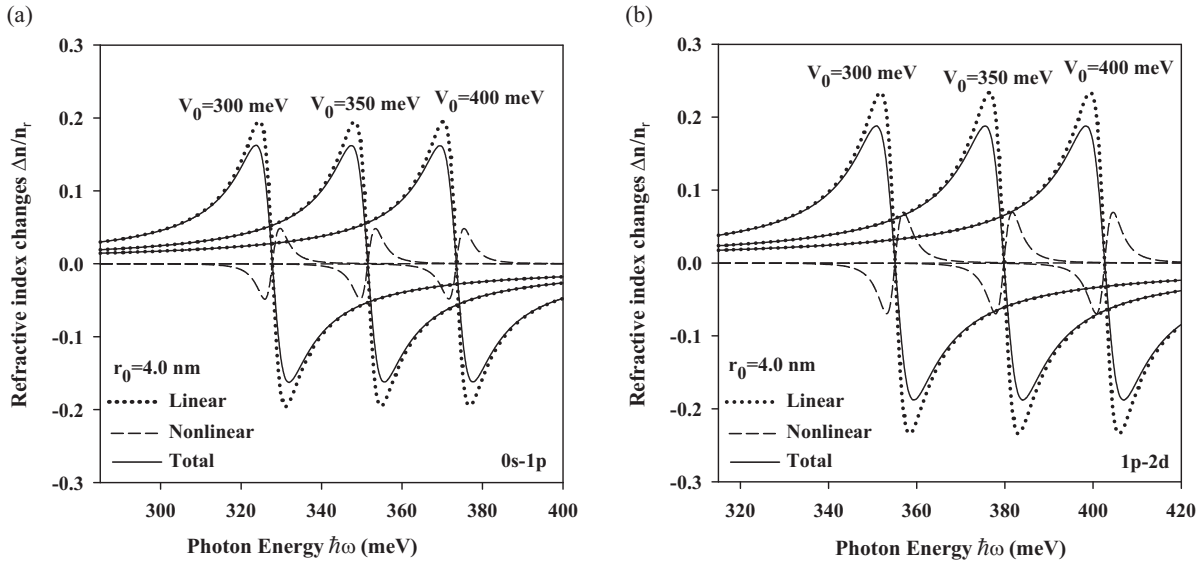

Fig. 6. Variation of the RICs as a function of the photon energy with different values of the chemical potential ($V_0 = 300$, 400, and 500 meV) at $r_0 = 5.0$ nm, $r = 7.0$ nm, and $I = 0.6\,\mathrm{MW/cm^2}$ for (a) $0s-1p$ and (b) $1p-2d$ transitions.

nant peak splits up into two separate peaks known as bleaching effect [36]. This is due to the negative contribution of the third-order nonlinear term. The resonant peak is significantly split up into two peaks due to the strong bleaching effect and this bleaching effect can be clearly observed when $I = 0.5\,\mathrm{MW/cm^2}$ for $0s-1p$ and $I = 0.4\,\mathrm{MW/cm^2}$ for $1p-2d$. This intensity value decreases when the transitions occur between the higher energy states. Figures 2–4 show that we may adjust the resonance conditions of the optical absorption by r_0, V_0, and I parameters.

The RICs are other important parameters in the optical studies of QDs. The variation of the RIC as a function of the photon energy with the zero point parameters is presented in Figure 5 at $V_0 = 300$ meV, $r = 7.0$ nm, and $I = 0.6\,\mathrm{MW/cm^2}$ for $0s-1p$ and $1p-2d$. It is obvious that the largest change in the total refractive index is contributed by the linear term. On the other hand, the nonlinear term is opposite of sign of the linear term. Thus, the change in the total refractive index will be reduced. As r_0 increases, the maximum values of RICs, though slightly, decrease and the maxima of the refractive index move toward lower energies (red shift) due to the same reason discussed in Figure 2. Similarly, the amplitudes of the RICs for $1p-2d$ are much stronger than that of $0s-1p$. We can also say that the total change in RICs is almost constant as r_0 increases for both $0s-1p$ and $1p-2d$ transitions.

Figure 6 presents the dependence of the RIC as a function of the photon energy with the chemical potential at $r_0 = 5.0$ nm, $r = 7.0$ nm, and $I = 0.6\,\mathrm{MW/cm^2}$ for $0s-1p$ and $1p-2d$. The confinement effects on the carriers motion increase and thus the energy difference between the electronic states increases with V_0. Therefore, the magnitude of the RIC increases and its peak moves to the larger energy regions, with the increment of V_0. From this figure, it is noted that the chemical potential does not considerably affect the peak value of the RICs. As seen from Figures 5 and 6, we can conclude that the variation of the RICs for $0s-1p$ and $1p-2d$ transitions strongly depends on r_0 and V_0 parameters.

4. Conclusion

We have studied theoretically the binding energies of ground state and excited states, the linear, nonlinear, and total ACs and the RICs for $0s-1p$ and $1p-2d$ in a spherical GaAs pseudodot system. The determination of the energy levels and their wave functions has been done within the effective-mass approximation, using the variational calculations. We have found that the binding energies decrease with the minimum value of the pseudoharmonic potential r_0 and they depend strongly on r_0, especially in the $1p$ and $2d$ states. The calculated results show that the optical absorption

spectra and the RICs are affected by r_0 and V_0. The resonant peaks both of the optical ACs and RICs are red shifted with increasing r_0, while their resonant peaks are blue shifted with increasing V_0. In addition, the amplitudes of the ACs and RICs for $1p-2d$ are much stronger than that of $0s-1p$. We hope that the present theoretical results could stimulate and guide more experimental studies and have a significant influence on improvements of optical devices.

In this study, we have investigated the electronic and optical properties of one electron in a spherical GaAs pseudodot. However, these properties for two interacting electrons in this system have not been examined. It would be most interesting to see what similarities and differences occur between these two systems. In addition, it is possible to consider other effects on the system such as electric field, magnetic field, hydrostatic pressure and temperature, polaron effect, etc.

[1] N. P. Montenegro and S. T. P. Merchancano, Phys. Rev B. **46**, 9780 (1992).
[2] C. Bose and C. K. Sarkar, Solid State Electron. **42**, 1661 (1998).
[3] I. F. I. Mikhail and I. M. M. Ismail, Phys. Stat. Sol. (b) **244**, 3647 (2007).
[4] S. Yilmaz, H. Safak, R. Sahingoz, and M. Erol, Cent. Eur. J. Phys. **8**, 438 (2010).
[5] C. Bose, J. Appl. Phys. **83**, 3089 (1998).
[6] C. Bose, Physica E **4**, 180 (1999).
[7] S. Baskoutas, A. F. Terzis, and E. Voutsinas, J. Comput. Theor. Nanos. **1**, 315 (2004).
[8] J.-H. Yuan and C. Liu, Physica E **41**, 41 (2008).
[9] W. Xie, Superlattice Microst. **46**, 693 (2009).
[10] W. Xie, Physica B **403**, 2828 (2008).
[11] A. Gharaati and R. Khordad, Superlattice Microst. **48**, 276 (2010).
[12] D. Loss and D. P. DiVincenzo, Phys. Rev. A **57**, 120 (1998).
[13] A. D. Yoffe, Adv. Phys. **50**, 1 (2001).
[14] Y. Masumoto and T. Takagahara, Semiconductor Quantum Dots, Springer, Berlin 2002.
[15] D. Heiss, M. Kroutvar, J. J. Finley, and G. Abstreiter, Solid State Commun. **135**, 591 (2005).
[16] V. A. Harutyunyan, E. M. Kazryan, A. A. Kostanyan, and H. A. Sarkisyan, Physica E **36**, 114 (2007).
[17] I. Karabulut and S. Baskoutas, J. Appl. Phys. **103**, 73512 (2008).
[18] W. Xie, Physica B **403**, 4319 (2008).
[19] B. Cakir, Y. Yakar, A. Ozmen, M. O. Sezer, and M. Sahin, Superlattice Microst. **47**, 556 (2010).
[20] Y. Yakar, B. Cakir, and A. Ozmen, Optics Commun. **283**, 1795 (2010).
[21] M. Kirak, S. Yilmaz, M. Sahin, and M. Gencaslan, J. Appl. Phys. **109**, 94309 (2011).
[22] S. Erkoc and R. Sever, Phys. Rev. A **37**, 2686 (1988).
[23] G. C. Maitland, M. Righby, E. B. Smith, and W. A. Wakeham, Intermolecular Forces, Oxford University Press, Oxford 1987.
[24] M. Sage and J. Goodisman, Am. J. Phys. **53**, 350 (1985).
[25] R. Khordad, Solid State Sci. **12**, 1253 (2010).
[26] G. Rezaei, Vaseghi, F. Taghizadeh, M. R. K. Vahdani, and M. J. Karimi, Superlattice Microst. **48**, 450 (2010).
[27] G. Rezaei, B. Vaseghi, R. Khordad, and H. Azadi Kenary, Physica E **43**, 1853 (2011).
[28] Y. B. Yu and H. J. Wang, Superlattice Microst. **50**, 252 (2011).
[29] W. Xie and S. Liang, Physica B **406**, 4657 (2011).
[30] W. Xie and Y. Chen, Superlattice Microst. **50**, 691 (2011).
[31] R. Khordad, Physica B **406**, 620 (2011).
[32] A. Cetin, Phys. Lett. A **372**, 3852 (2008).
[33] R. Sever, C. Tezcan, M. Aktas, and O. Yesiltas, J. Math. Chem. **43**, 845 (2008).
[34] A. Ozmen, Y. Yakar, B. Cakir, and U. Atav, Optics Commun. **282**, 3999 (2009).
[35] R. Khordad, Int. J. Theor. Phys. **52**, 837 (2013).
[36] D. Ahn and S. L. Chuang, IEEE J. Quantum Electron. **23**, 2196 (1987).